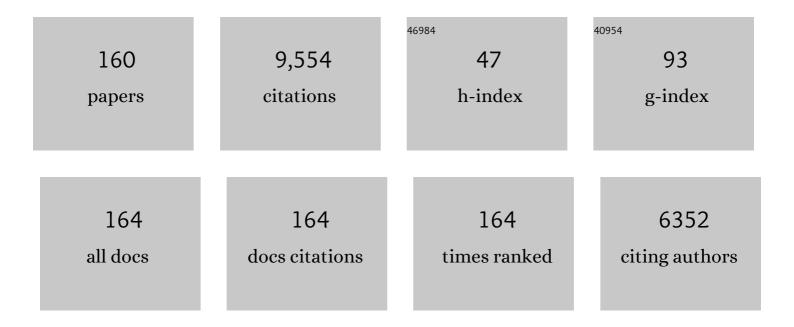
Gang Sha

List of Publications by Year in descending order

Source: https://exaly.com/author-pdf/2319007/publications.pdf Version: 2024-02-01



CANC SHA

#	Article	IF	CITATIONS
1	Effects of arsenic on the distribution and mode of occurrence of gold during fluid-pyrite interaction: A case study of pyrite from the Qiucun gold deposit, China. American Mineralogist, 2022, 107, 914-929.	0.9	10
2	Application of atom probe tomography in understanding high entropy alloys: 3D local chemical compositions in atomic scale analysis. Progress in Materials Science, 2022, 123, 100854.	16.0	21
3	A new dynamic recrystallization mechanism in adiabatic shear band of an α/β dual phase titanium alloy: Composition redistribution. Scripta Materialia, 2022, 206, 114229.	2.6	16
4	Synergistic effects of Cd, Si and Cr additions on precipitation strengthening and thermal stability of dispersoids in AA3003 alloy. Materials Science & Engineering A: Structural Materials: Properties, Microstructure and Processing, 2022, 832, 142422.	2.6	5
5	Formation of high-temperature inner oxide scale on low alloy steels: Segregation, partitioning and transformation reactions. Corrosion Science, 2022, 195, 109980.	3.0	5
6	Rapid dislocation-mediated solute repartitioning towards strain-aging hardening in a fine-grained dilute magnesium alloy. Materials Research Letters, 2022, 10, 21-28.	4.1	17
7	Ion-irradiation-induced clustering in Fe-Mn-Ni-(Si) steels: Nucleation, growth and chemistry evolution. Journal of Nuclear Materials, 2022, 560, 153477.	1.3	1
8	Effects of atom probe analysis parameters on composition measurement of precipitates in an Al-Mg-Si-Cu alloy. Ultramicroscopy, 2022, 235, 113495.	0.8	6
9	Uniting tensile ductility with ultrahigh strength via composition undulation. Nature, 2022, 604, 273-279.	13.7	80
10	Temperature-dependent-composition of η phase in an Al-Zn-Mg-Cu alloy under high pressure torsion: Kinetics and thermodynamics. Acta Materialia, 2022, 237, 118181.	3.8	6
11	Mechanically Reinforced Artificial Enamel by Mg ²⁺ -Induced Amorphous Intergranular Phases. ACS Nano, 2022, 16, 10422-10430.	7.3	8
12	Composition-dependent dynamic precipitation and grain refinement in Al-Si system under high-pressure torsion. Journal of Materials Science and Technology, 2021, 68, 199-208.	5.6	16
13	Enhancement of strength-ductility balance of heavy Ti and Al alloyed FeCoNiCr high-entropy alloys via boron doping. Journal of Materials Science and Technology, 2021, 75, 154-163.	5.6	42
14	Precipitation kinetics and morphology evolution of the Co3(Al, W) phase in a medium supersaturation Co–Al–W alloy. Journal of Materials Science, 2021, 56, 2597-2611.	1.7	4
15	Longitudinal wave attenuation in polycrystals with elongated grains: 3D numerical and analytical modeling. Journal of the Acoustical Society of America, 2021, 149, 2377-2394.	0.5	14
16	Effect of cobalt on precipitation in Fe-Cr-Co-Mo-Ni-C stainless steels. Materials Letters, 2021, 289, 129439.	1.3	1
17	A medium-range structure motif linking amorphous and crystalline states. Nature Materials, 2021, 20, 1347-1352.	13.3	92
18	Enhanced tensile properties in a Cu-Al2O3 alloy via trace Ti addition. Journal of Alloys and Compounds, 2021, 862, 158687.	2.8	13

#	Article	IF	CITATIONS
19	Ultrastrong nanocrystalline oxide-dispersion-strengthened ferritic alloy with exceptional thermal stability. Materials Science & Engineering A: Structural Materials: Properties, Microstructure and Processing, 2021, 821, 141616.	2.6	12
20	Temperature-Dependent Irradiation-Induced Clustering in a Fe–Mn–Ni Alloy. Metallurgical and Materials Transactions A: Physical Metallurgy and Materials Science, 2021, 52, 4264-4274.	1.1	3
21	Inversion methodology for ultrasonic characterization of polycrystals with clusters of preferentially oriented grains. Ultrasonics, 2021, 115, 106433.	2.1	11
22	Origins of high ductility exhibited by an extruded magnesium alloy Mg-1.8Zn-0.2Ca: Experiments and crystal plasticity modeling. Journal of Materials Science and Technology, 2021, 84, 27-42.	5.6	39
23	Stabilizing a severely deformed Al–7Mg alloy with a multimodal grain structure via Mg solute segregation. Journal of Materials Science and Technology, 2021, 89, 141-149.	5.6	31
24	A new mechanism of surface phase formation on precipitation-hardening alloy under ion irradiation. Applied Surface Science, 2021, 563, 150358.	3.1	2
25	Shearing and rotation of β″ and βʹ precipitates in an Al-Mg-Si alloy under tensile deformation: In-situ and ex-situ studies. Acta Materialia, 2021, 220, 117310.	3.8	46
26	Prominent role of multi-scale microstructural heterogeneities on superplastic deformation of a high solid solution Al–7Mg alloy. International Journal of Plasticity, 2021, 146, 103108.	4.1	38
27	Tailoring microstructure of metallic glass for delocalized plasticity by pressure annealing: Forward and inverse studies. Acta Materialia, 2021, 220, 117282.	3.8	8
28	Irradiation-induced segregation/desegregation at grain boundaries of a ferritic Fe-Mn-Si steel. Acta Materialia, 2021, 220, 117297.	3.8	16
29	Irradiation-induced clustering in a Fe-Mn-Si alloy at different doses and temperatures. Journal of Nuclear Materials, 2021, 557, 153237.	1.3	4
30	Self-inhibition effect of metal incorporation in nanoscaled semiconductors. Proceedings of the National Academy of Sciences of the United States of America, 2021, 118, .	3.3	0
31	Nanoscale pathways for human tooth decay – Central planar defect, organic-rich precipitate and high-angle grain boundary. Biomaterials, 2020, 235, 119748.	5.7	26
32	Formation of solute nanostructures in an Al–Zn–Mg alloy during long-term natural aging. Journal of Alloys and Compounds, 2020, 821, 153572.	2.8	33
33	Atom Probe Tomography Characterization of Dopant Distributions in Si FinFET: Challenges and Solutions. Microscopy and Microanalysis, 2020, 26, 36-45.	0.2	1
34	Bulk nanocrystalline high-strength magnesium alloys prepared via rotary swaging. Acta Materialia, 2020, 200, 274-286.	3.8	134
35	Efficient Er/Oâ€Doped Silicon Lightâ€Emitting Diodes at Communication Wavelength by Deep Cooling. Advanced Optical Materials, 2020, 8, 2000720.	3.6	23
36	Direct Imaging of Liquid–Nanoparticle Interfaces with Atom Probe Tomography. Journal of Physical Chemistry C, 2020, 124, 19389-19395.	1.5	13

#	Article	IF	CITATIONS
37	Maximizing the accuracy of finite element simulation of elastic wave propagation in polycrystals. Journal of the Acoustical Society of America, 2020, 148, 1890-1910.	0.5	21
38	Ultrastrong low-carbon nanosteel produced by heterostructure and interstitial mediated warm rolling. Science Advances, 2020, 6, .	4.7	75
39	Revealing Solute Clusters in Coalescence by Atom Probe Tomography Analysis. Microscopy and Microanalysis, 2020, 26, 1079-1087.	0.2	2
40	Attenuation and velocity of elastic waves in polycrystals with generally anisotropic grains: Analytic and numerical modeling. Journal of the Acoustical Society of America, 2020, 147, 2442-2465.	0.5	26
41	Solute-dislocation interactions and creep-enhanced Cu precipitation in a novel ferritic-martensitic steel. Acta Materialia, 2020, 195, 199-208.	3.8	60
42	Enhanced nucleation and precipitation hardening in Al–Mg–Si(–Cu) alloys with minor Cd additions. Materials Science & Engineering A: Structural Materials: Properties, Microstructure and Processing, 2020, 792, 139698.	2.6	18
43	Elastic wave velocity dispersion in polycrystals with elongated grains: Theoretical and numerical analysis. Journal of the Acoustical Society of America, 2020, 148, 3645-3662.	0.5	13
44	Influence of aging pathways on the evolution of heterogeneous solute-rich features in peak-aged Al-Mg-Si-Cu alloy with a high Mg/Si ratio. Philosophical Magazine Letters, 2019, 99, 49-56.	0.5	4
45	The Microstructural Characterization of NiSi-Rich Sub-precipitates Within Cementite in Isothermally Aged Reactor Pressure Vessel Steel. Metallurgical and Materials Transactions A: Physical Metallurgy and Materials Science, 2019, 50, 3992-3999.	1.1	2
46	Improvement of grain boundary tolerance by minor additions of Hf and B in a second generation single crystal superalloy. Acta Materialia, 2019, 176, 109-122.	3.8	45
47	Phase stability of an high-entropy Al-Cr-Fe-Ni-V alloy with exceptional mechanical properties: First-principles and APT investigations. Computational Materials Science, 2019, 170, 109161.	1.4	15
48	Gradient Microstructures and Mechanical Properties of Ti-6Al-4V/Zn Composite Prepared by Friction Stir Processing. Materials, 2019, 12, 2795.	1.3	9
49	Segregation and precipitation at grain boundaries of weathering steels without/with Sb addition. Materials Chemistry and Physics, 2019, 236, 121783.	2.0	9
50	Solute clustering and precipitation in an Al–Cu–Mg–Ag–Si model alloy. Materials Science & Engineering A: Structural Materials: Properties, Microstructure and Processing, 2019, 760, 366-376.	2.6	22
51	Strengthening mechanisms in an ultrafine-grained Al Zn Mg Cu alloy processed by high pressure torsion at different temperatures. Materials Science & Engineering A: Structural Materials: Properties, Microstructure and Processing, 2019, 752, 223-232.	2.6	34
52	Precipitation strengthening in an ultralight magnesium alloy. Nature Communications, 2019, 10, 1003.	5.8	88
53	Atom Probe Tomography Analysis of TiCx Powders Synthesized by SHS in Al/Fe/Cu–Ti–C Systems. Materials, 2019, 12, 4095.	1.3	4
54	Influence of Zn on the distribution and composition of heterogeneous solute-rich features in peak aged Al-Mg-Si-Cu alloys. Scripta Materialia, 2019, 159, 5-8.	2.6	44

Gang Sha

#	Article	IF	CITATIONS
55	Understanding formation of Mg-depletion zones in Al-Mg alloys under high pressure torsion. Journal of Materials Science and Technology, 2019, 35, 858-864.	5.6	14
56	Dynamic precipitation, segregation and strengthening of an Al-Zn-Mg-Cu alloy (AA7075) processed by high-pressure torsion. Acta Materialia, 2019, 162, 19-32.	3.8	166
57	Solute clustering in Al-Mg-Si-Cu-(Zn) alloys during aging. Journal of Alloys and Compounds, 2019, 774, 347-363.	2.8	53
58	On the atomic model of Guinier-Preston zones in Al-Mg-Si-Cu alloys. Journal of Alloys and Compounds, 2018, 745, 644-650.	2.8	18
59	Effect of extrusion temperature on microstructure and properties of an ultrafine-grained Cu matrix nanocomposite fabricated by powder compact extrusion. Journal of Materials Science, 2018, 53, 5389-5401.	1.7	19
60	Numerical and analytic modelling of elastodynamic scattering within polycrystalline materials. Journal of the Acoustical Society of America, 2018, 143, 2394-2408.	0.5	38
61	Universal scaling of transverse wave attenuation in polycrystals. Ultrasonics, 2018, 88, 84-96.	2.1	12
62	Enhanced inter-diffusion of immiscible elements Fe/Cu at the interface of FeZr/CuZr amorphous multilayers. Materials Research Letters, 2018, 6, 55-60.	4.1	12
63	Effects of temperature on the irradiation responses of Al0.1CoCrFeNi high entropy alloy. Scripta Materialia, 2018, 144, 31-35.	2.6	103
64	High temperature stabilization of a nanostructured Cu-Y2O3 composite through microalloying with Ti. Materials Science & Engineering A: Structural Materials: Properties, Microstructure and Processing, 2018, 712, 80-87.	2.6	35
65	Ultrastrong nanocrystalline steel with exceptional thermal stability and radiation tolerance. Nature Communications, 2018, 9, 5389.	5.8	88
66	Understanding structural evolution of nanostructured Cu-Al2O3 composite powders during thermomechanical processing. Materialia, 2018, 4, 268-275.	1.3	9
67	High-content ductile coherent nanoprecipitates achieve ultrastrong high-entropy alloys. Nature Communications, 2018, 9, 4063.	5.8	399
68	Segregation induced hardening in annealed nanocrystalline Ni-Fe alloy. Materials Science & Engineering A: Structural Materials: Properties, Microstructure and Processing, 2018, 735, 354-360.	2.6	19
69	Enhanced dispersoid precipitation and dispersion strengthening in an Al alloy by microalloying with Cd. Acta Materialia, 2018, 157, 114-125.	3.8	79
70	Nucleation driving force for ω-assisted formation of α and associated ω morphology in β-Ti alloys. Scripta Materialia, 2018, 155, 149-154.	2.6	31
71	The effects of microalloying on the precipitate microstructure at grain boundary regions in an Mg-Zn-based alloy. Materials and Design, 2017, 119, 290-296.	3.3	29
72	Finite-element modelling of elastic wave propagation and scattering within heterogeneous media. Proceedings of the Royal Society A: Mathematical, Physical and Engineering Sciences, 2017, 473, 20160738.	1.0	53

Gang Sha

#	Article	IF	CITATIONS
73	Iron in solution with aluminum matrix after non-equilibrium processing: an atom probe tomography study. Philosophical Magazine Letters, 2017, 97, 118-124.	0.5	7
74	Si-induced precipitation modification and related age-hardening response of an Al–4Mg–1Cu–0.5Si alloy. Materials Chemistry and Physics, 2017, 193, 421-426.	2.0	8
75	Grain boundary stability governs hardening and softening in extremely fine nanograined metals. Science, 2017, 355, 1292-1296.	6.0	572
76	Non-uniform phase separation in ferrite of a duplex stainless steel. Acta Materialia, 2017, 140, 388-397.	3.8	49
77	Microstructural origins of high strength and high ductility in an AlCoCrFeNi2.1 eutectic high-entropy alloy. Acta Materialia, 2017, 141, 59-66.	3.8	501
78	Entropy as a Geneâ€Like Performance Indicator Promoting Thermoelectric Materials. Advanced Materials, 2017, 29, 1702712.	11.1	218
79	Effect of Pre-strain on the Solute Clustering, Mechanical Properties, and Work-Hardening of a Naturally Aged Al-Cu-Mg Alloy. Metallurgical and Materials Transactions A: Physical Metallurgy and Materials Science, 2017, 48, 4121-4134.	1.1	6
80	Bauschinger Effect and Back Stress in Gradient Cu-Ge Alloy. Metallurgical and Materials Transactions A: Physical Metallurgy and Materials Science, 2017, 48, 3943-3950.	1.1	32
81	High-entropy Al0.3CoCrFeNi alloy fibers with high tensile strength and ductility at ambient and cryogenic temperatures. Acta Materialia, 2017, 123, 285-294.	3.8	378
82	Sensitivity Analysis of Laser Effect on Mg-Gd-Er Alloy. Microscopy and Microanalysis, 2017, 23, 714-715.	0.2	0
83	Microstructural evolution and phase transformation in twinning-induced plasticity steel induced by high-pressure torsion. Acta Materialia, 2016, 109, 300-313.	3.8	58
84	The role of ω in the precipitation of Î \pm in near-Î ² Ti alloys. Scripta Materialia, 2016, 117, 92-95.	2.6	37
85	Quantitative measurement for the microstructural parameters of nano-precipitates in Al-Mg-Si-Cu alloys. Materials Characterization, 2016, 118, 352-362.	1.9	41
86	Atomic-scale homogenization in an fcc-based high-entropy alloy via severe plastic deformation. Journal of Alloys and Compounds, 2016, 686, 15-23.	2.8	23
87	New insights into the phase transformations to isothermal ω and ω-assisted α in near β-Ti alloys. Acta Materialia, 2016, 106, 353-366.	3.8	155
88	Precipitation hardening of an Mg–5Zn–2Gd–0.4Zr (wt. %) alloy. Acta Materialia, 2016, 108, 207-218.	3.8	70
89	Microstructural evolution, strengthening and thermal stability of an ultrafine-grained Al–Cu–Mg alloy. Acta Materialia, 2016, 109, 202-212.	3.8	163
90	Corrosion Behaviour of Al–4Mg–1Cu (wt%) Microalloyed with Si and Ag. Advanced Engineering Materials, 2015, 17, 1670-1674.	1.6	4

#	Article	IF	CITATIONS
91	The influence of partitioning on the growth of intragranular α in near-β Ti alloys. Journal of Alloys and Compounds, 2015, 643, 212-222.	2.8	39
92	Strengthening of an Al–Cu–Mg alloy processed by high-pressure torsion due to clusters, defects and defect–cluster complexes. Materials Science & Engineering A: Structural Materials: Properties, Microstructure and Processing, 2015, 627, 10-20.	2.6	70
93	Age-hardening effect and formation of nanoscale composite precipitates in a NiAlMnCu-containing steel. Materials Science & Engineering A: Structural Materials: Properties, Microstructure and Processing, 2015, 627, 340-347.	2.6	39
94	Enhanced bake-hardening response of an Al–Mg–Si–Cu alloy with Zn addition. Materials Chemistry and Physics, 2015, 162, 15-19.	2.0	48
95	Far-field scattering model for wave propagation in random media. Journal of the Acoustical Society of America, 2015, 137, 2655-2669.	0.5	34
96	The mechanism of ï‰-assisted α phase formation in near β-Ti alloys. Scripta Materialia, 2015, 104, 75-78.	2.6	75
97	A high-specific-strength and corrosion-resistant magnesium alloy. Nature Materials, 2015, 14, 1229-1235.	13.3	561
98	Mechanisms for enhanced plasticity in magnesium alloys. Acta Materialia, 2015, 82, 344-355.	3.8	119
99	Atomistic structure of Cu-containing β″ precipitates in an Al–Mg–Si–Cu alloy. Scripta Materialia, 2014, 75, 86-89.	2.6	63
100	Precipitation of the α-phase in an ultrafine grained beta-titanium alloy processed by severe plastic deformation. Materials Science & Engineering A: Structural Materials: Properties, Microstructure and Processing, 2014, 605, 144-150.	2.6	22
101	Strength, grain refinement and solute nanostructures of an Al–Mg–Si alloy (AA6060) processed by high-pressure torsion. Acta Materialia, 2014, 63, 169-179.	3.8	123
102	Microscopy and microanalysis of complex nanosized strengthening precipitates in new generation commercial Al–Cu–Li alloys. Journal of Microscopy, 2014, 255, 128-137.	0.8	28
103	Effect of solution treatment on precipitation and age-hardening response of an Al–4Mg–1Cu–0.5Si–0.4Ag (wt%) alloy. Materials Science & Engineering A: Structural Materials: Properties, Microstructure and Processing, 2014, 599, 64-68.	2.6	8
104	Analysis of strengthening in AA6111 during the early stages of aging: Atom probe tomography and yield stress modelling. Acta Materialia, 2013, 61, 7285-7303.	3.8	142
105	Precipitation of quasicrystal approximant phases in an Al–Mg–Cu–Ge alloy. Philosophical Magazine Letters, 2013, 93, 77-84.	0.5	5
106	Confined Auâ€₽d Ensembles in Mesoporous TiO ₂ Spheres for the Photocatalytic Oxidation of Acetaldehyde. ChemCatChem, 2013, 5, 3557-3561.	1.8	18
107	Solute clustering and solute nanostructures in an Al–3.5Cu–0.4Mg–0.2Ge alloy. Acta Materialia, 2013, 61, 3724-3734.	3.8	39
108	Enhanced age-hardening response of Al–4Mg–1Cu (wt.%) microalloyed with Ag and Si. Scripta Materialia, 2013, 68, 857-860.	2.6	30

#	Article	IF	CITATIONS
109	Influence of experimental parameters on the composition of precipitates in metallic alloys. Ultramicroscopy, 2013, 132, 199-204.	0.8	5
110	Influence of Low Level Ag Additions on Mgâ€Alloy AZ91. Advanced Engineering Materials, 2013, 15, 485-490.	1.6	9
111	Effects of Si addition on the microstructure evolution of Al–Cu–Mg alloys in the α + S + T Philosophical Magazine Letters, 2013, 93, 648-654.	phase fiel	d. ₁₂
112	Influence of heat treatment on the microstructure, texture and formability of 2024 aluminium alloy. Materials Science & Engineering A: Structural Materials: Properties, Microstructure and Processing, 2012, 552, 48-60.	2.6	85
113	Enhanced grain refinement of an Al–Mg–Si alloy by high-pressure torsion processing at 100°C. Materials Science & Engineering A: Structural Materials: Properties, Microstructure and Processing, 2012, 552, 415-418.	2.6	43
114	Heterogeneous nucleation of β-type precipitates on nanoscale Zr-rich particles in a Mg-6Zn-0.5Cu-0.6Zr alloy. Nanoscale Research Letters, 2012, 7, 300.	3.1	8
115	Hydrogen-induced decomposition of Zr-rich cores in an Mgâ^'6Znâ^'0.6Zrâ^'0.5Cu alloy. Acta Materialia, 2012, 60, 5615-5625.	3.8	26
116	A New Approach to the Determination of Concentration Profiles in Atom Probe Tomography. Microscopy and Microanalysis, 2012, 18, 359-364.	0.2	40
117	Solute nanostructures and their strengthening effects in Al–7Si–0.6Mg alloy F357. Acta Materialia, 2012, 60, 692-701.	3.8	132
118	Precipitation microstructure and age-hardening response of an Mg–Gd–Nd–Zn–Zr alloy. Materials Science & Engineering A: Structural Materials: Properties, Microstructure and Processing, 2012, 534, 1-6.	2.6	21
119	Precipitation microstructure and their strengthening effects of an Mg–2.8Nd–0.6Zn–0.4Zr alloy with a 0.2 wt.% Y addition. Materials Science & Engineering A: Structural Materials: Properties, Microstructure and Processing, 2012, 538, 272-280.	2.6	15
120	Effects of isothermal annealing on the microstructures and mechanical properties of a FeCuSiBAl amorphous alloy. Materials Science & Engineering A: Structural Materials: Properties, Microstructure and Processing, 2012, 543, 145-151.	2.6	19
121	Towards new aluminium alloys through advances in atom probe microscopy. , 2012, , 29-30.		0
122	Microstructure and mechanical properties of Mg–6Zn–xCu–0.6Zr (wt.%) alloys. Journal of Alloys and Compounds, 2011, 509, 3526-3531.	2.8	48
123	Mechanical behaviors of as-deposited and annealed nanostructured Ni–Fe alloys. Scripta Materialia, 2011, 65, 1-4.	2.6	33
124	Solute segregation and texture modification in an extruded magnesium alloy containing gadolinium. Scripta Materialia, 2011, 65, 919-921.	2.6	207
125	Segregation of solute elements at grain boundaries in an ultrafine grained Al–Zn–Mg–Cu alloy. Ultramicroscopy, 2011, 111, 500-505.	0.8	107
126	A comparison of the structure of solute clusters formed during thermal ageing and irradiation. Ultramicroscopy, 2011, 111, 664-671.	0.8	48

#	Article	IF	CITATIONS
127	Nanostructure of aluminium alloy 2024: Segregation, clustering and precipitation processes. Acta Materialia, 2011, 59, 1659-1670.	3.8	191
128	Elemental redistribution in a nanocrystalline Ni–Fe alloy induced by high-pressure torsion. Materials Science & Engineering A: Structural Materials: Properties, Microstructure and Processing, 2011, 528, 7500-7505.	2.6	8
129	Precipitation and solute clustering in aluminium: advanced characterisation techniques. , 2011, , 345-366.		4
130	Precipitation Process in Mg-Nd-Zn-Zr-Gd/Y Alloy. , 2011, , 255-259.		0
131	Solute clustering in Al–Cu–Mg alloys during the early stages of elevated temperature ageing. Acta Materialia, 2010, 58, 4923-4939.	3.8	189
132	Effect of Al and Gd Solutes on the Strain Rate Sensitivity of Magnesium Alloys. Metallurgical and Materials Transactions A: Physical Metallurgy and Materials Science, 2010, 41, 734-743.	1.1	91
133	Microstructural evolution of Fe-rich particles in an Al–Zn–Mg–Cu alloy during equal-channel angular pressing. Materials Science & Engineering A: Structural Materials: Properties, Microstructure and Processing, 2010, 527, 4742-4749.	2.6	38
134	Hardening and microstructural reactions in high-temperature equal-channel angular pressed Mg–Nd–Gd–Zn–Zr alloy. Materials Science & Engineering A: Structural Materials: Properties, Microstructure and Processing, 2010, 527, 5092-5099.	2.6	30
135	Evolution of solute clustering in Al–Cu–Mg alloys during secondary ageing. Acta Materialia, 2010, 58, 1795-1805.	3.8	102
136	An atom probe characterisation of grain boundaries in an aluminium alloy processed by equal-channel angular pressing. International Journal of Materials Research, 2009, 100, 1674-1678.	0.1	23
137	Determining the composition of small features in atom probe: bcc Cu-rich precipitates in an Fe-rich matrix. Ultramicroscopy, 2009, 109, 535-540.	0.8	66
138	Atom Probe Tomography of Solute Distributions in Mg-Based Alloys. Metallurgical and Materials Transactions A: Physical Metallurgy and Materials Science, 2009, 40, 2480-2487.	1.1	29
139	Effect of laser pulsing on the composition measurement of an Al–Mg–Si–Cu alloy using three-dimensional atom probe. Ultramicroscopy, 2009, 109, 580-584.	0.8	30
140	Influence of equal-channel angular pressing on precipitation in an Al–Zn–Mg–Cu alloy. Acta Materialia, 2009, 57, 3123-3132.	3.8	253
141	Field evaporation behavior during irradiation with picosecond laser pulses. Applied Physics Letters, 2008, 92, .	1.5	58
142	Partitioning and segregation of trace element Sn in a low-alloy steel. Philosophical Magazine Letters, 2007, 87, 327-339.	0.5	10
143	Overview: Recent Progress in Three-Dimensional Atom Probe Instruments and Applications. Microscopy and Microanalysis, 2007, 13, 408-417.	0.2	46
144	Atom probe tomography today. Materials Today, 2007, 10, 36-42.	8.3	216

#	Article	IF	CITATIONS
145	Thermal Ageing Effect of Pressure Vessel Steels. , 2006, , .		1
146	Comparison of the number densities of nanosized Cu-rich precipitates in ferritic alloys measured using EELS and EDX mapping, HREM and 3DAP. Journal of Materials Science, 2006, 41, 2559-2565.	1.7	18
147	Characterization of Fe-Rich Intermetallic Phases in a 6xxx Series Al Alloy. Materials Science Forum, 2006, 519-521, 1721-1726.	0.3	23
148	Characterization of Segregation and Precipitation at Grain Boundaries in Thermally Aged Pressure Vessel Steels. , 2006, , .		0
149	Trace Element Sn Segregation in Cu-rich Precipitates during Thermal Ageing of Pressure Vessel Steels. , 2006, , .		0
150	Kinetic Monte Carlo simulation of clustering in an Al–Zn–Mg–Cu alloy (7050). Acta Materialia, 2005, 53, 907-917.	3.8	86
151	Field ion microscopy and 3-D atom probe analysis of Al3Zr particles in 7050 Al alloy. Ultramicroscopy, 2005, 102, 151-159.	0.8	38
152	Characterization of precipitates in an aged 7xxx series Al alloy. Surface and Interface Analysis, 2004, 36, 564-568.	0.8	44
153	Early-stage precipitation in Al–Zn–Mg–Cu alloy (7050). Acta Materialia, 2004, 52, 4503-4516.	3.8	646
154	Quasi-peritectic solidification reactions in 6xxx series wrought Al alloys. Acta Materialia, 2003, 51, 1883-1897.	3.8	69
155	Growth related metastable phase selection in a 6xxx series wrought Al alloy. Materials Science & Engineering A: Structural Materials: Properties, Microstructure and Processing, 2001, 304-306, 612-616.	2.6	64
156	The effect of layer number on the superplasticity of laminate 7475/2091Al alloy. , 2000, 35, 2711-2718.		3
157	Effect of Grain Refiner on Intermetallic Phase Formation in Directional Solidification of 6xxx Series Wrought Al Alloys. Materials Science Forum, 2000, 331-337, 253-258.	0.3	21
158	Rotational transitions of N2(a 1Îg) induced by collisions with Ar/He and N2(a 1Îg)–N2(X 1Σ+g) ro energy transfer studied by laser REMPI spectroscopy. Journal of Chemical Physics, 1987, 87, 5251-5255.	vibronic 1.2	22
159	Rovibronic energy transfer from N2(a 1ï€g) to CO(A 1ï€) studied by laser REMPI spectroscopy. Journal of Chemical Physics, 1987, 87, 2742-2749.	1.2	21
160	Effect of Thermal Aging on Microstructural Evolution in Ferrite of Duplex Stainless Steel in Nuclear Power Plant Applications. Materials Science Forum, 0, 898, 818-825.	0.3	0